Macromolecules

Article

pubs.acs.org/Macromolecules

From 1D Rods to 3D Networks: A Biohybrid Topological Diversity Investigated by Asymmetrical Flow Field-Flow Fractionation

Susanne Boye,[†] Franka Ennen,[†,‡] Linda Scharfenberg,[†,‡] Dietmar Appelhans,*[,†] Lars Nilsson,*[,§] and Albena Lederer*[,†,‡]

[†]Leibniz-Institut für Polymerforschung Dresden e.V., Hohe Straße 6, 01069 Dresden, Germany

[‡]Technische Universität Dresden, 01062 Dresden, Germany

[§]Food Colloids Group and Lund Center for Field-Flow Fractionation, Department of Food Technology, Engineering and Nutrition, Faculty of Engineering LTH, Lund University, Lund, Sweden

Supporting Information

ABSTRACT: Biohybrid structures formed by noncovalent interaction between avidin as a bridging unit and biotinylated glycodendrimers based on poly(propyleneimine) (GD-B) have potential for biomedical application. Therefore, an exact knowledge about molar mass, dispersity, size, shape, and molecular structure is required. Asymmetrical flow field-flow fractionation (AF4) was applied to separate pure and assembled macromolecules according to their diffusion coefficients. The complex biohybrid structures consist of single components (avidin, differently valent GD-B) and nanostructures. These nanostructures were systematically studied depending on the degree of biotinylation and ligand−receptor stoichiometry by AF4 in combination with dynamic and static light scattering detection. This enables the quantification of composition and calculation of molar masses and radii, which were used to analyze scaling properties and apparent density of the formed structures. These data are compared to hydrodynamic radii obtained by applying the retention theory to the AF4 data. It is shown that depending on their architecture the molecular shape of biohybrid structures is changed from rod-like to spherical toward network-like behavior.

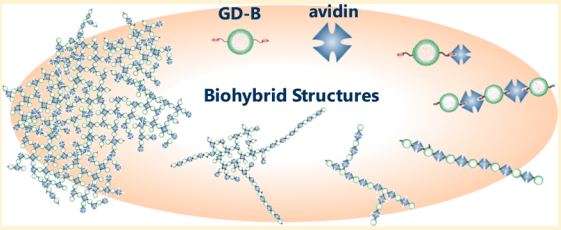

1. INTRODUCTION

An exact knowledge about molar mass, dispersity, size, shape, and molecular structure is essential for complex systems, especially in the case of controlled interactions between synthesized polymers and natural proteins. These structures have a high potential for application as nanoelectronic devices, artificial enzymes, and biosensors as well as in the field of photonics and biomedicine.[1−4] The modification of polymers with biological ligands or receptors facilitates the specific interactions. Caused by the high noncovalent binding strength ($K_d = 10^{-15}$ M), the avidin−biotin conjugation has gained great interest not only to fabricate well-defined biohybrid and supramolecular structures for delivery and sensor systems but also to build up protein-containing polymer films with sensor properties.[5,6]

A recent development is directed to create water-soluble, well-defined smaller or larger, nanometer-sized biohybrid structures. They consist of avidin as central, linear, and branching unit and biotinylated glycodendrimers (fourth generation of poly(propyleneimine) PPI-G4 as a core molecule) decorated with a dense maltose shell (DS, >90% of the surface amino groups are substituted) and fabricated by polymeric association reactions. The formation of defined biohybrid structures is strongly triggered by the number and the spacer length (PEG spacer or shorter alkyl spacer) of biotin ligands and the ligand−receptor stoichiometry of glycodendrimers (GD-B$_x$, x = 0, 1, 2, etc.) and avidin.[7] However, there is still a lack of deeper knowledge of their molecular parameters (size, molar mass, shape, density, etc.). These unknown facts are of major interest to understand the structure−property relationship in different environments for future biomedical applications.

Different characterization techniques are applied for the determination of size, molar masses, or other molecular parameters.[8−15] Though, without a separation of the single components, the information is limited to average values without knowledge on the size and molar mass distribution of these multicomponent biohybrid structures.

Generally, molecular or aggregate sizes, molecular structure, and composition of biohybrids or natural polymers are evaluated by molar mass dependencies determined by light scattering techniques after sample separation.[16,17] However, commonly used size exclusion chromatography (SEC) is not suitable for different reasons, e.g., adsorptive interactions of multifunctional polymers with the column material[18−20] or coelution caused by limited separation range.[21] Additionally,

Received: April 19, 2015
Revised: June 1, 2015
Published: June 16, 2015

DOI: 10.1021/acs.macromol.5b00824
Macromolecules 2015, 48, 4607−4619

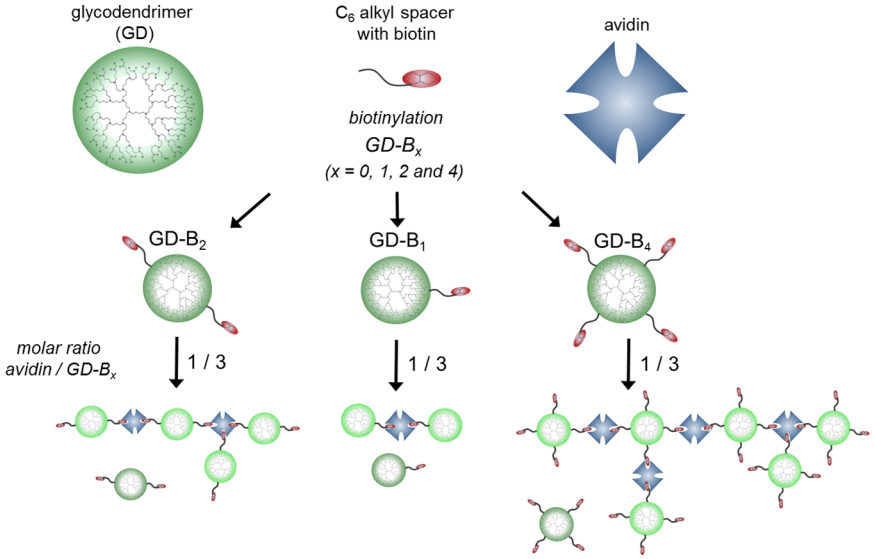

Figure 1. Schematic overview of initial components (glycodendrimer, spacered biotin ligand, and avidin) and idealized examples for the formation of biohybrid structures by differently biotinylated glycodendrimers. Taking into account that not all four binding sites in avidin can be occupied due to steric requirement of participating biotinylated glycodendrimers during biohybrid formation.[7]

SEC does not allow a gentle separation due to strong and destructive shear forces.[22] A powerful alternative to SEC is asymmetrical flow field-flow fractionation (AF4) combined with light scattering (LS). In contrast to liquid chromatography, AF4 separation does not occur in a stationary phase but in a flat, long channel. This minimizes the adsorptive loss of samples. Furthermore, reduced pressure and shear forces provide a gentle separation with minimized degradation of structures based on noncovalent interactions. Depending on diffusion coefficients, the samples are transported and separated by a laminar, axial flow.[23] The use of AF4 enables a characterization of a broad range of complex architectures especially for conjugated, multicomponent systems.[24−29] Subsequent reliable detection with a concentration sensitive detector (refractive index (RI) or UV−vis) and a multiangle light scattering detector (MALS) could enable full information about composition, molar masses, radius of gyration (R_g), and geometry distributions.[30,31]

Coupled to AF4, the online dynamic light scattering (DLS) is gaining in importance for the determination of diffusion coefficient (D) distributions. There is an increasing number of studies in which AF4-DLS was applied for the characterization.[32−39] Advantages of online AF4-DLS measurements are the determination of the hydrodynamic radius (R_h) distributions and the high molecular and structural information density (scaling properties, apparent density, and ratio between R_g and R_h related to molar mass distribution). Thus, this analytical method can be used without sample purification or fractionation, which is sometimes necessary for batch measurements. Furthermore, in the case of using the DLS as add-on unit of a MALS detector the scattering angle θ and scattering vector q can be varied easily for optimizing the scattering intensity. The R_h can be calculated by applying the Stokes−Einstein equation[40]

$$R_h = \frac{Tk_B}{6\pi\eta D} \tag{1}$$

where T is the temperature, k_B is the Boltzmann constant, η is the dynamic viscosity of the solvent, and D is the diffusion coefficient.

There are also some drawbacks of online DLS. DLS in flow is challenging in the low concentration regions of fractionation or at low diffusion coefficients (large analytes), for which longer correlation times are needed. Hence, the separation methods have to be adapted e.g. by using higher sample loads or especially for larger macromolecules by decreasing or stopping the detector flow (R_h > 50 nm).[41] Not at least, acquisition costs should be taken into account.

As initially mentioned, AF4 in normal elution mode is based on separation according to differences in the diffusion coefficients. Hence, AF4 interpretation using the retention theory can deliver directly D and R_h distribution from the retention time (t_R) by combining Stokes−Einstein (eq 1)[40] and retention theory:[42]

$$R_h = \frac{t_R k_B T}{\pi\eta w^2 (F_x/F_c)} \tag{2}$$

where k_B is the Boltzmann constant, T is the absolute temperature, η is the dynamic viscosity of the solvent, w is the channel thickness, and F_x/F_c is the ratio of the cross-flow rate F_x to the channel flow rate F_c.

R_h can be directly calculated from t_R as it was done for spherical particles like e.g. liposomes.[43] This calculation becomes more complex if the cross-flow changes during elution. A numerical solution based on the classical retention theory was developed for the mostly used trapezoidal channel design[44] and was improved for decaying cross-flow using eq 3:[45,46]

$$\frac{dz_i}{dt_R} = f(F_x) D_i k \tag{3}$$

where z_i is the position of sample component i along the channel and k is a constant comprising geometrical parameters of the channel and flow conditions. Equation 3 is a simplified and highly condensed expression of the full differential equation. Reliable and accurate calculation of data requires

DOI: 10.1021/acs.macromol.5b00824
Macromolecules 2015, 48, 4607−4619

precisely determined channel geometry and height as well as flow rates.[45,47] Furthermore, it should be considered that calculation is limited to elution in normal mode. The largest benefit of this calculation is the additional profit of information without applying dynamic light scattering. Diffusion coefficients can be calculated as long as no coelution occurs and its concentration is high enough for detection. Recently, several studies have been performed based on the classical retention theory in order to determine the R_h and further structural information.[32,48,49]

Our work is focused on comprehensive studies of various biohybrid structures formed by GD-B_x and avidin by using AF4 coupled with MALS and/or DLS. In this context, a comparison between different approaches of the determination of analyte radii will be presented, and advantages and limits will be discussed. Thus, a detailed overview on the molecular shape and distribution of biohybrid structures (Figure 1) as a function of molar masses and degree of biotinylation is given.

2. EXPERIMENTAL PART AND MATERIAL DETAILS

Glycodendrimers and Biohybrid Systems. Dendritic polymers (monovalent GD-B_1, bivalent GD-B_2, and tetravalent GD-B_4) have been used from a previous study[7] which describes the synthesis, characterization, and the determination for the number of biotin ligands of biotinylated GD by HABA displacement assay in detail. For a better understanding of the complexity of the topic, we focus on GD macromolecules which possess C_6-alkyl spacers to connect the biotin with the surface of the dendritic scaffold. Figure 1 summarizes schematically the different biohybrid structures dependent on the number of biotin ligands and the ligand−receptor stoichiometry of GD-B_x. Detailed structure of the glycoarchitectures of GD-B_1, GD-B_2 and GD-B_4 are presented in the Supporting Information (Figure SI 1).

Sample Preparation. Deionized, UV-treated, and ultrafiltered water (Purelab Plus UV/UF equipment, USF Elga, DE) water was used to prepare the eluent 0.05 M $NaNO_3$, pH 6.9 with addition of 0.02% sodium azide (w/v) to prevent bacteria growth.

Analyses of bioconjugates were performed 3 days after mixing of individual biotinylated glycodendrimers and avidin solutions with a concentration of 1 mg/mL.

Determination of Refractive Index Increment (d*n*/d*c*). For M_w determination with LS the dn/dc values were externally determined at 25 °C using Optilab T-rEX (Wyatt Technology Europe GmbH, Germany). Different sample concentrations in the range of 0.1 and 2.5 mg/mL were prepared for this purpose. 900 μL was injected manually into the flow cell. The calculation of dn/dc values was performed by Astra 5.3.4.20 software (Wyatt Technologies, USA).

Refractive index increments in $NaNO_3$ solution are 0.2085 mL/g for PPI-G4, 0.174 mL/g for avidin, 0.140 mL/g for GD, 0.143 mL/g for GD-B_1, 0.145 mL/g for GD-B_2 and GD-B_4, and 0.160 mL/g for the avidin/GD-B_x associates (x = 1, 2, or 4) at different molar ratios.

Asymmetrical Flow Field-Flow Fractionation. AF4 measurements were performed to determine the molar masses of pure and biotinylated GD and bioconjugates with an Eclipse Dualtec system (Wyatt Technology Europe, Germany) with 0.05 M $NaNO_3$ and 0.02% (w/v) NaN_3 as carrier liquid. The channel spacer made of poly(tetrafluoroethylene) (PTFE) had a thickness of 490 μm, and the channel dimensions were 26.5 cm in length and from 2.1 to 0.6 cm in width.

The membranes used as accumulation wall were composed of regenerated cellulose (RC) with a molecular weight cutoff (MWCO) of 10 kDa (Superon GmbH, Germany). For the measurements of PPI-G4 a MWCO of 5 kDa was applied. Flow rates were controlled with an Agilent Technologies 1200 series isocratic pump equipped with vacuum degasser. The detection system consists of a MALS detector (DAWN HELEOS II, Wyatt Technology Europe, Germany) operating at a wavelength of 690 nm with online DLS detector (DynaPro NanoStar, Wyatt Technologies, USA) which is an add-on unit connected to the 99° angle of the MALS and a refractive index (RI) detector (Optilab T-rEX, Wyatt Technology Europe GmbH, Germany) operating at a wavelength of 658 nm. The angle for DLS was chosen due to high baseline scattering at lower and higher angles. All injections were performed with an autosampler (1260 series, Agilent Technologies Deutschland GmbH). The channel flow rate (F_c) was maintained at 1.0 mL/min for all standard AF4 operations. In the case of online DLS experiments of the initial components F_c was decreased to 0.8 mL/min and for the bioconjugates to 0.2 mL/min. If not mentioned otherwise, the focus flow (F_f) was set at 3 mL/min for 2 min. In the case of focus dependency tests the flow rate and time were varied. Each fractogram presented is representative of triplicate sample measurements and shows the elution phase subsequent to focus mode starting directly after the switch from focus to elution phase.

In general, the injection volume was 50 μL in the case of single components (glycodendrimers and avidin) and bioconjugates with a sample concentration of 1 g/L. In the case of concentration dependency tests the injection volume and sample concentrations were varied. For online DLS measurements the sample load was increased up to 300 μg (300 μL of a 1 mg/mL solution) to prevent data scattering. Overloading effects are not taken into account since they do not influence the R_h data are obtained.

Unless otherwise stated, the cross-flow rate (F_x) during the elution step was optimized by a linear F_x gradient of 3 to 0.1 mL/min in 15 min for the single components and the bioconjugates in order to enable a direct comparison of fractograms (separation method A). For online DLS experiments of the initial components the optimized F_x gradient was 2.3 to 0.1 mL/min in 20 min with an additional isocratic flow step applying F_x of 0.1 mL/min (separation method B). For the bioconjugates the separation method was adapted to F_c of 0.2 mL/min and a linear F_x gradient 1 to 0.08 mL/min in 15 min with additional isocratic F_x of 0.08 mL/min for an additional 20 min (separation method C). The isocratic F_x of 0.08 mL/min has not been generated but flow rate of 0 mL/min was adjusted by the system, due to system limits at low flow rates caused by low cross-flow pressure below the membrane. After 15 min of elution the F_x decreases to 0 mL/min while the F_c increases to 0.28 mL/min.

Collecting and processing of detector data were made by the Astra software, version 6.1.1.17 (Wyatt Technology, USA). The molar mass dependence of retention time was fitted in most cases with fourth degree exponential for differential distributions. Lowest and highest scattering angles have been neglected. The scattering results for biohybrid structures above 500 kg/mol have been calculated according to Berry plot due to a accurate data fit for molar masses.[50]

Deconvolution of peaks of initial components in biohybrid systems was done in Origin software version 9.0 and calculation of molar mass distribution by results of Astra software.

The determination of R_h from retention times was performed by using the Stokes−Einstein equation (1), and the diffusion coefficient was obtained by the application retention theory eqs 2 and 3 according to ref 45. The calculation was performed in a MatLab based software developed and provided by the Food Colloids Group at Lund University, Sweden. The focus point was determined by bromophenol blue measurement, and the channel thickness (w = 426 μm) was calculated form the retention time of bovine serum albumin (BSA) standard (Sigma-Aldrich, Germany) measurement[46] using the monomer peak with a hydrodynamic diameter of 7.7 nm.

Dynamic Light Scattering (DLS) in Batch. DLS measurements were carried out with a WYATT DynaPro NanoStar (Wyatt Technologies, USA), working with a 658 nm laser. It allows dynamic light scattering detection (90°) in batch mode in a temperature range from −15 to 150 °C. The avalanche photodiode collects data in 100 ns intervals; evaluation of the acquired data was performed with DYNAMICS-Software (Wyatt Technologies, USA). The sample concentration was about 1 mg/mL.

DOI: 10.1021/acs.macromol.5b00824
Macromolecules 2015, 48, 4607−4619

Table 1. Results of Analysis with AF4-MALS-DLS and DLS in Batch of Initial Components

components	M_{theor} (kg/mol)	$M_{w,total}$ (kg/mol)	$Đ_{total}$ (M_w/M_n)	recovery (%)	$M_{w,main\ peak}$ (kg/mol)	$R_{h,online}$ [c] (nm)	$R_{h,calc}$ [d] (nm)	$R_{h,batch}$ (nm)
PPI-G4[a]	7.17	9.5	1.05	61	8.7	–[b]	–[b]	–[b]
GD	47.9	50.4	1.05	87	48.3	3.4 ± 0.2	3.4 ± 0.01	3.1 ± 0.2
GD-B_1	48.2	57.1	1.14	92	49.3	2.8 ± 0.1	2.7 ± 0.01	2.8 ± 0.2
avidin	66	75.3	1.09	91	68.2	2.9 ± 0.1	2.7 ± 0.01	3.1 ± 0.2

[a]Measurements are performed with RC membrane (MWCO 5 kDa). [b]Not determined. [c]Separation method B with reduced F_c and increased sample load. [d]Calculated according to retention theory.

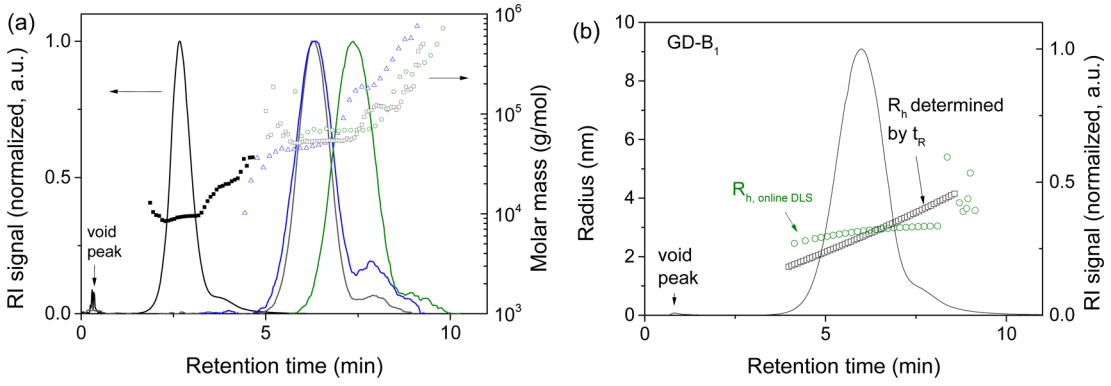

Figure 2. AF4 fractograms: (a) solid line (represents RI signals) and symbols (represent molar masses) of PPI dendrimer (filled black square), glycodendrimer (GD, open square), biotinylated glycodendrimer GD-B_1 (blue triangle), and avidin (green circle) during elution mode using method A; (b) AF4 RI signal of GD-B_1 as a function of differently determined R_h (black squares: by retention times; green circles: by online DLS) using separation method B.

3. RESULTS AND DISCUSSION

Characterization of the Initial Components. The understanding of the formation of biohybrid structures presupposes the accurate molar mass determination of the initial components. A separation of glycodendrimers with SEC leads to a nonreversible adsorption inside of the column due to their densely branched structure and the high number of functional groups in the dendritic structure comparable to other dendritic glycopolymers as observed in our previous studies.[25,51] For this reason, AF4-MALS-DLS was chosen as a suitable alternative for molar mass determination. In the first step the initial components such as the PPI dendrimer (fourth generation), the non-biotinylated glycodendrimer GD, the monovalent (GD-B_1) as representative for GD-B_x, and the protein avidin were measured with separation method A (described in the Experimental section). Distinction of differently biotinylated GD is not possible due to marginal change in molar masses, which cannot be detected with this method. The obtained results of AF4 experiments are listed in Table 1.

The experimental data of the main peaks show a good correlation with the theoretical values, and the recovery of all measurements is between 87 and 92%, except the initial PPI dendrimer. This could be due to a loss of low molecular fractions of PPI trough the membrane. Additionally, the cationic amino groups can interact with the slightly negatively charged membrane surface.[52] The higher R_h of GD compared to GD-B_1 can be explained by the synthetic pathway described in ref 7. The coupling step of the biotin ligands in the case of GD-B_x is performed on the initial PPI-G4 followed by a maltosylation step (see Supporting Information, Figure SI 1). Compared to GD, the absolute number of maltose units of GD-B_1 is lower.[7] A distribution of biotin ligands leads to a decrease of maltose units and consequentially lower average R_h values.

The fractograms (see Figure 2a) show a bimodal peak shape for the initial components. The monovalent GD-B_1 is plotted as a representative for all GD-B_x. All peaks possess a minor shoulder at higher retention times corresponding to higher molar masses. In the case of avidin the high molar mass shoulder has a very low concentration. The amount in this part, calculated from peak area, is less than 4% of mass of the entire peak. For the initial dendrimer PPI this part can be quantified to 7% of mass and for the non-biotinylated GD to 5%. With increasing biotin number the amount of the high molar mass shoulder increases from 14% of mass for GD-B_1 to 22% for GD-B_4.

The molar masses of the main peak at lower retention times (see Figure 2a) have narrow dispersities (M_w/M_n) lower than 1.01, which is typical for dendrimers. Furthermore, the molar masses of this main peak show a very good agreement with the expected values (see Table 1). The small shoulder at higher retention times corresponds exactly to multiples of single macromolecules. For PPI-G4, GD, and GD-B_x the molar mass was 2-fold and for avidin 3-fold. The high molecular fraction of the protein can be explained by the aggregation of avidin monomers into dimers and trimers. For the glycodendrimers aggregation can be excluded; otherwise, broader distributions would have been observed. The AF4-LS measurement of PPI-G4 also showed a shoulder with higher molar masses. This observation and the reproducibility of this exact (multiple) increase after modification with maltose and biotin ligands, leading to the assumption that the initial dendrimer sample consists of a minor fraction of two linked dendrimer macromolecules. No influence of focus time and/or flow or concentration on this shoulder was observed.

Furthermore, a comparison between R_h values determined by online DLS and by retention times is shown in Figure 2b. The flow profile was adjusted in order to obtain reliable online DLS data and to reduce data scattering. The channel and cross-flow

DOI: 10.1021/acs.macromol.5b00824
Macromolecules 2015, 48, 4607–4619

rates are reduced with almost unchanged ratio of F_x/F_c, and the sample load is increased as described in the Experimental section. The longer acquisition times enable an accurate determination of sizes. Though, both methods lead to different R_h curves: online DLS only provide an almost constant curve with a marginal increase in low concentration region at higher retention times (8−10 min), while the radii calculated from theory exhibit a lower starting value and a steeper slope. This deviation can be explained by the different determination approaches. Theoretically, dendrimers exhibit a monodisperse distribution—the size should remain constant with the retention time as observed by online DLS. The small fraction (at about 8 min) of larger R_h, visible in the fractogram and molar mass curve, cannot be detected due to low sample amount within this fraction which is less than 4% of detected total mass (concentration ≤0.01 mg/mL). Hence, online DLS does not yield reliable results in the low concentration region. The application of the high channel height in order to increase the separation efficiency leads to slight band broadening. These marginally broader signals influence the calculation by means of retention theory. Generally, retention theory calculates size dependency on retention time and cannot take into account band broadening. Thus, in the case of monodisperse dendrimers slight deviations arise when the R_h is calculated from retention theory. Nevertheless, the deviations as a function of retention time do not influence the resulting mean values. In summary, it can be stated that the observed deviations of differently determined average R_h of the initial components are only marginal (less than 4%). Another contribution to the deviations observed originates from the optimization of conditions necessary for online DLS, leading to unnecessary band broadening caused by low flow rates.

The average value of R_h (determined by online DLS) is in the same size range in comparison to the calculated R_h and measured R_h by DLS in batch (see Table 1) for all initial components. The three different strategies (online DLS, batch DLS, and determination from t_R) for the size determination lead to comparable results. This is valid, especially in the case of narrowly distributed components with small size.

Formation of Biohybrid Structures. For the formation of biohybrid structures (meaning defined bioconjugation adducts as well smaller/larger nanostructures) the number of avidin-available biotin ligands plays an important role. The main focus is to characterize stable structures of mono-, bi-, and tetravalent GD-B by AF4-LS in order to obtain reliable information about the conformational properties. The intention was to generate biohybrid structures with tunable sizes according to the degree of biotinylation and varied ligand−receptor stoichiometry as described in ref 7. From the theoretical point of view, the involved avidin and GD-B_x can act as different structure units (terminal, linear, and branching units)[7] in the corresponding biohybrid structures, shortly indicated in Figure 1. Thus, GD-B_1 with only one biotin ligand as terminal unit should generate conjugation adducts with diameters of approximately 15−20 nm, while avidin acts as central unit. Whereas, multivalent GD having two or more biotin groups at the surface should be able to form larger structures. In this case, the substituted GD-B_2 can act as a linear unit, while GD-B_4 and avidin are available as linear or as branching units generating complex biohybrid structures. In the bioconjugation process of multivalent GD and avidin, avidin can also act as linear and branching units, too. Later in this work it will be discussed which participating macromolecules in the biohybrid structure formation can dominate the generation of branching units. These branching units are essential for the formation of various nanostructures.

Dynamic Light Scattering in Batch. Dynamic light scattering measurements in batch were performed to obtain a first insight into the sample characteristics prior to AF4 studies. Biohybrid structures are prepared by variation of the molar ratio of protein/dendrimer (equimolar and 3-fold excess of GD-B_x) and the available, spacered biotin molecules (degree of biotinylation). Stable bioconjugates were obtained at least 3 days after mixing of initial components. The long formation time is caused by the steric effects of the spacer between GD and biotin and the geometry of the binding pockets of avidin.[7] Correspondingly, AF4 measurements of the freshly mixed bioconjugates show low reproducibility. Time-dependent DLS measurements of the mixture confirm an increase in the stability with increasing conjugation time (see Supporting Information, Figure SI 2).

The DLS measurements of single components can be applied very accurately due to low dispersities (see Table 1). The results are comparable to R_h obtained by online DLS (described in Characterization of the Initial Components section). In contrast, the investigations of different biohybrid systems indicate a multimodal distribution with fractions consisting of different components. One fraction was identified in all systems, which contains small macromolecules in the dimensions of the single, initial macromolecules. At least one further fraction contains macromolecules with larger radii (see Supporting Information, Figure SI 3). However, only average values can be obtained which are dependent on the applied fit of the autocorrelation function. In the case of an imprecise fitting the calculated "distribution" is not correct. Especially, when large biohybrid structures are present in the mixture, smaller macromolecules will be overlaid and the calculated values are overestimated. Hence, this multicomponent system requires a separation in combination with adequate detection systems to obtain qualitative (identification of components) and quantitative (composition of mixture) information.

AF4 Separation of Biohybrid Structures: Identification and Quantification of Components. An optimized AF4 separation is essential for an accurate and comprehensive characterization of the biohybrid structures. This includes the best combination of sample parameters (concentration and sample load), channel parameters (e.g., thickness and geometry), and flow conditions.

Initial separation experiments by AF4 and the corresponding molar mass determination showed that increasing ligand−receptor stoichiometry increased the probability of occupied avidin binding sites.[7] To understand the formation of defined biohybrid structures (e.g., 1:3 composition between avidin and GD-B_1) and larger biohybrid structures mentioned as nanostructures here in this study, one should bear in mind that the determined number of biotin in GD-B_x (x = 1, 2, or 4) is only an average value of biotin ligands in the corresponding GD-B_x. These mean values are obtained by HABA titrations (see Supporting Information, Figure SI 4).[7] This implies that GD-B_x possesses a distribution of biotin ligands. One preconsideration is that GD-B_1 can also form nanostructures because additionally to GD-B_1 as a main component, also GD with 0, 2, 3, and 4 biotin ligands in lower amounts are also present. The distribution can be described analogous to a Poisson distribution as observed in ref 53. Similar assumptions can be made for GD-B_2 and GD-B_4. Moreover, the biotin ligands in GD-B_x are statistically distributed on the PPI-G4 surface after the synthesis of the precursors for GD-B_x (see

DOI: 10.1021/acs.macromol.5b00824
Macromolecules 2015, 48, 4607−4619

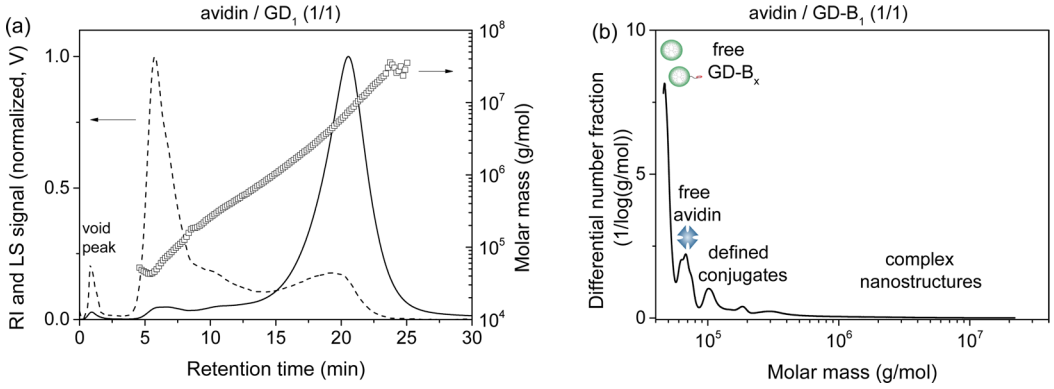

Figure 3. (a) AF4 fractogram (method A) with LS signal (solid line), RI signal (dashed line), and molar masses (symbols) and (b) molar mass distribution of bioconjugates formed by avidin and GD-B_1 in equimolar ratio (1/1) with schematic structure assignment.

Supporting Information, Figure SI 1). It is assumed that biotin ligands are separated with maximal distance to each other in GD-B_x. The assumption is also supported by other results from interaction studies.[54−56]

The chosen AF4 separation enables the complete elution of the sample within the elution mode. For each biohybrid sample, the separation profile shows multimodality that indicates an inhomogeneous composition of the mixture comprising of larger structures together with the well-defined architectures. The identification of all components was performed by subdivision of the different peaks and the calculation of molar masses according to our first AF4 studies.[7] The AF4 measurements enable a comprehensive overview of the molar masses, sizes, and compositions of biohybrid structures (Supporting Information, Table SI 1−3).

In the following part, the composition of biohybrid structures formed by monovalent GD-B_1 is exemplarily discussed. As observed in our previous studies, an equimolar ratio (1:1) of avidin and GD-B_1 leads to a broadly distributed, multimodal peak (Figure 3a), where the different components can be clearly identified (Figure 3b) and quantified (Supporting Information, Table SI 1). The fractions consist of (i) free, nonbonded GD$_x$ and nonconverted avidin, (ii) defined conjugation adducts with stoichiometry of one and three GD-B_1 attached to avidin, and (iii) low amount of broadly distributed, large and complex biohybrid architectures (nanostructures) formed by multivalent GD in GD-B_1 sample.

A complete conversion of avidin is achieved and the fraction of free avidin disappears when the amount of GD-B_1 is increased to a 3-fold excess compared to avidin. Furthermore, the amount of free, nonconverted GD-B_x is strongly increased. Simultaneously, the second fraction of defined conjugation adducts with avidin as central unit (Figure 1) possesses completely occupied avidin macromolecules calculated by protein/GD-B_x stoichiometry (Supporting Information, Table SI 1). Surprisingly, this result indicates that the existence of completely occupied binding pockets of avidin *is possible*, but with low content (Supporting Information, Table SI 1) compared to other components in the analyzed conjugation solution. The reason for low content for 1 to 4 association structures can be explained by the large steric requirement of glycodendrimer GD-B_1 with respect to similar size dimension of avidin as postulated in our former study.[7] Moreover this supports our working hypothesis that avidin can act as branching unit in identified nanostructures (Figure 3) when at least three binding pockets in avidin are occupied by three biotin ligands. In addition, the size and molar masses of nanostructures increase using 3-fold excess of GD-B_1 (Supporting Information, Table SI 1).

These results can be verified for GD-B with higher degree of biotinylation. In case of the bi- and tetravalent GD-B the same conjugation behavior is observed compared to GD-B_1. For equimolar ratio and 3-fold excess of GD-B_x (Supporting Information, Tables SI 2 and SI 3), GD-B_x and avidin are found in the mixture in addition to defined biohybrids and nanostructures. Exemplarily, in the case of GD-B_4 defined conjugation adducts consist of two avidin and three GD-B_4 macromolecules, while these biohybrid structures can be considered as linear and/or branching building blocks in the formation of larger nanostructures (Supporting Information, Table SI 3). Moreover, the presence of multivalent GD-B_x (x = 2 or 4) gives the opportunity to overcome the steric effect of biotinylated glycodendrimers with respect to avidin binding capacity[7] to the multivalent GD-B_x (x = 2 or 4). Thus, avidin is always the decisive parameter in the formation of linear chains or structures (Figure 4). However, a branching unit inside the biohybrid structures is also needed, which can lead to a higher amount and larger sizes of the complex nanostructures with a suspected (high) density of branching (Supporting Information, Tables SI 2 and SI 3). The postulation that avidin is the decisive parameter in the formation of larger nanostructures is directed to specific association and dissociation process of avidin against pure biotin ligand. It was postulated that the cis-position of two biotin ligands in the binding pockets of avidin preferentially undergoes a transformation process into a trans-position of biotin ligands.[57] Such processes can also be assumed to occur during the formation of smaller and larger biohybrid structures. This fact explains why the formation process of biohybrid structures needs at least 3 days to be completed. Moreover, we cannot exclude that multivalent GD-B can also act as branching unit (Figure 4). Clarification for this point can be solved by future theoretical calculations.

Scaling Properties of Biohybrid Structures Depending on Size and Composition. Biohybrid Structures Based on GD-B1. The described AF4 separation experiments of the bioconjugate systems indicate a complex relation between composition of initial solution and size of the formed biohybrid structures. The determination of molecular dimension like R_h and R_g provides detailed information about the scaling properties in relation to molar masses. In our studies, we compare different strategies to obtain specific radii. R_g is calculated using the data obtained by AF4-MALS. R_h is determined by two different approaches

DOI: 10.1021/acs.macromol.5b00824
Macromolecules 2015, 48, 4607−4619

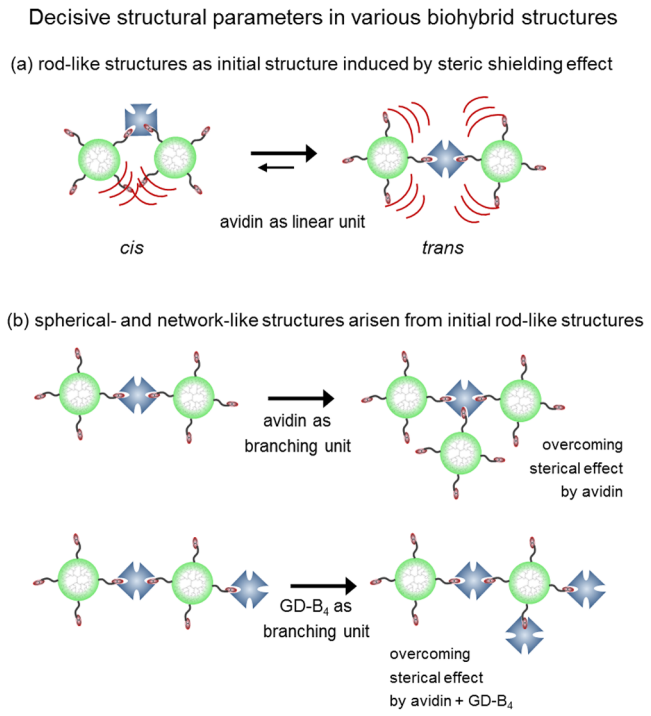

Figure 4. Schematic overview of *assumed structural components* for the formation of various biohybrid structures ((a) rod-like and (b) spherical- and network-like) considered as nanostructures. At the moment for the spherical- and network-like structures avidin is even more the decisive key parameter for the formation of branching units compared to multivalent GD-B_x (x = 2 or 4) due to intra- and intermolecular dissociation and association processes between avidin and GB-B_x.[7]

(online AF4-DLS and by t_R). The AF4 separation method was adapted to determine accurate values of R_h by online DLS (separation methods B and C, Experimental section). Low sample loads resulted in high scattering of the data due to low fraction concentrations. An increase of injected sample led to an identical trend in R_h determined by retention times (Supporting Information, Figure SI 9), but higher radii were detected because of the higher concentration of large biohybrid structures. The average R_h is increased from 15.8 nm (40 μg sample load) up to 22.4 nm (200 μg sample load) shown for biohybrid structures formed by avidin/GD-B_2 (1/1) as an representative example for all other structures. For further optimization the channel (detector) flow and cross-flow rate was reduced to improve the acquisition times and the fit of autocorrelation function, respectively.

As an example, the fractograms and radii of biohybrid structures formed by avidin/GD-B_1 (1/3) are shown in Figure 5a. For lower molar masses determination of R_g is not possible due to limitations in light scattering theory (i.e., isotropic scattering). The direct comparison within the fractogram (Figure 5a) reveals a very good correlation of R_h determined by DLS and calculation of R_h from retention times. After 20 min, the slope of all radii changes when the F_x gradient is completed, and the F_x is constant (0.1 mL/min) for the remaining measurement time. The same behavior can be observed for all investigated biohybrid systems. Possible explanations of this effect could be the low sample amount within this fraction (retention times >25 min) and the short acquisition time in flow DLS for the larger macromolecules. Consequently, the determined radii are underestimated. Similar behavior has been observed for polysaccharides.[33] In that study, the flow was stopped during the elution of large macromolecules to increase the acquisition time and to provide them enough time for detection of the Brownian motion. In order to achieve a similar effect, we strongly decreased the flow rate (0.2 mL/min), which will be discussed below.

The examination of the scaling properties can support the above assumptions. Figure 5b shows the dependency of molar masses on the differently determined radii that delivers information about the conformational properties in solution on a molecular level according to eq 4:[58]

$$R = KM^{\nu} \tag{4}$$

The scaling factor ν is characterized by the slope of this dependence and theoretically defined for a sphere $\nu \sim 0.33$ and for a random coil $\nu \sim 0.5-0.6$. The slope of both R_h curves is close to $\nu = 0.5$ in the region of defined conjugation adducts between 1×10^5 and 4×10^5 g/mol and is characteristic for coil-like structures with a high compactness. However, for this region the scaling factor as a function of R_g cannot be determined due to limitations in static light scattering theory (isotropic scattering). Only for $R_g > \sim 10$ nm reliable values can be obtained. In the region of nanostructures (above 5×10^5 g/mol), the trend ($\nu = 0.4$) of all conformation plots indicates nanostructures with more compact, sphere-like shape due to the low number of multivalent GD-B_x ($x > 1$), as previously

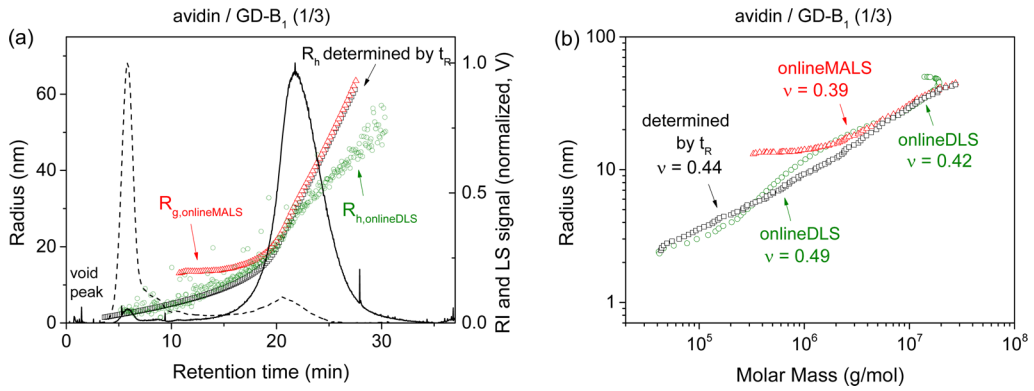

Figure 5. (a) AF4 fractograms (RI signal, dashed line; LS signal, solid line) with differently determined radii by online MALS (R_g, red triangles), by online DLS (R_h, green circles), and by retention times (R_h, black squares) and (b) conformation plot with differently determined radii as a function of molar mass with calculated scaling factors of biohybrid structures formed by avidin/GD-B_1 (1/3).

DOI: 10.1021/acs.macromol.5b00824
Macromolecules 2015, 48, 4607−4619

described, and the ability of avidin or GD-B$_x$ to act as a connection unit.

One further possibility to understand the molecular composition of the nanostructures is the ratio between R_g and R_h, $\rho = R_g/R_h$. This ratio gives valuable information about the conformation and shape especially about the molecular shape in relation to the molar mass distribution.[58]

Figure 6 shows the ρ parameters as a function of the molar mass. Both curves (of differently determined R_h) possess similar

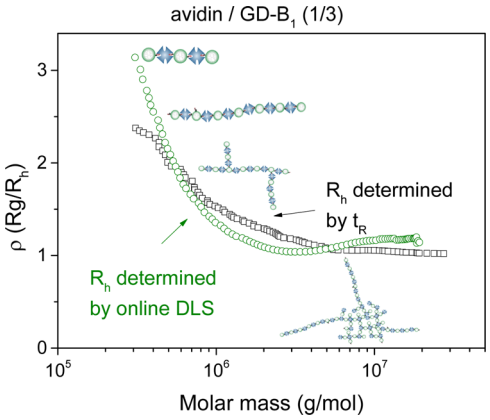

Figure 6. ρ parameter (R_g/R_h) vs molar mass, comparison of R_h determination by retention times (black squares) and by online DLS (green circles) of biohybrid structures formed by avidin/GD-B$_1$ (1/3).

trends characterized by a decreased ρ parameter with increasing molar masses. A high ρ parameter of 2.5 and 3 is calculated with differently determined R_h for the molar mass region of smaller, defined conjugation adducts. Such high values are typical for stiff rods, with a high axial ratio for instance found for xanthan gum in solution.[59] Up to a molar mass of 10^6 g/mol linear, rod-like chains are formed. Preferred steric location of GD-B on opposite binding sites of avidin is caused by very short linker (C_6 spacer) between rather large, sphere-like GD-B that binds to sphere-like avidin. Hence, the big size of the dendrimer and avidin in combination with short linker results in high persistence length and high stiffness of the short chains which prevents folding. These nonflexible, linear chains grow with higher degree of conjugation. One should keep in mind that the chain growth is also accompanied by dissociation and association processes between avidin and multivalent GD-B$_x$ (Figure 4). At a certain molar mass (10^6 g/mol), several two-dimensional branching points are generated as indicated by the ρ parameter of 1.5, which is typical for branched polymers.[58] When the biohybrid structures become larger and more complex, the ρ value decreases to 1 as typical for branched or star-like conformation. Obviously, these large nanostructures exhibit three-dimensional structure consisting of a very compact and branched core with several linear segments reaching into the outer surroundings ("star-like" structure).

It has to be considered that the structure transformation is not a time-dependent process. The entire biohybrid system consists of different structures simultaneously.

The determination of apparent density could provide additional information to understand variations in the ρ values. The apparent density over a size distribution is usually expressed by molar mass and R_g (eq 5).[60]

$$d_{\mathrm{app},i} = \frac{M_i}{V(R_g)_i N_A}\alpha \tag{5}$$

where M_i is the molar mass fraction i, V_i is the volume of fraction i, N_A is the Avogadro number, and α is a geometrical correction factor given by eq 6:

$$\alpha = \frac{V_{\mathrm{sphere}}(R_g)}{V_{\mathrm{sphere}}(R)} = \frac{{R_g}^3}{R^3} = \frac{\left(\sqrt{\frac{3}{5}}R\right)^3}{R^3} = \left(\frac{3}{5}\right)^{3/2} \tag{6}$$

The determined apparent density reveals a change in the compactness of the conjugation adducts (see Figure 7) with increasing molar masses toward nanostructures.

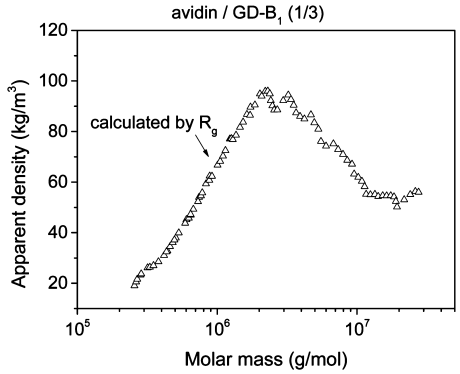

Figure 7. Apparent density vs molar mass, calculated using R_g by AF4-MALS (corrected with α) of biohybrid structures formed by avidin/GD-B$_1$ (1/3).

The calculated density increases with molar mass to values comparable to the densities calculated for casein micelles in milk.[49] At a certain size the structures become less dense but still cross-linked. This behavior is typical for aggregation or formation of network-like structures. Swollen hydrogel-like networks with less dense inner areas, filled with solvent molecules, typically exhibit such properties.

The interpretation of the apparent density together with the ρ parameter (Figure 6) and the scaling factor (Figure 5b) shows that with the molar mass increase a change in the supramolecular topology from less dense structure to compact branched structure up to approximately 2×10^6 g/mol is achieved. At higher molar masses these compact structures are coupled to each other by long, linear segments, which contribute to the decrease of the overall apparent density in the biohybrid network.

In order to get deeper insight into the large size region, better DLS detection of the components in this section was obtained by reducing the channel flow rate (Experimental section, separation method c). Here, the detection of higher sizes is enabled by increasing the sample amount as a result of lower flow velocities leading to a longer residence time in the detector (Supporting Information, Figure SI 10a). The separation efficiency is slightly decreased due longitudinal band broadening caused by the longer residence time in the separation channel. For this measurement no comparison with R_h from retention theory was possible as the instrumental step was unable to regulate the low constant F_x in the later stage of elution. This most likely originates from the low pressure in the channel when using the F_c = 0.2 mL/min (separation method C) as the instrumental setup relies on pressure-dependent

DOI: 10.1021/acs.macromol.5b00824
Macromolecules 2015, 48, 4607−4619

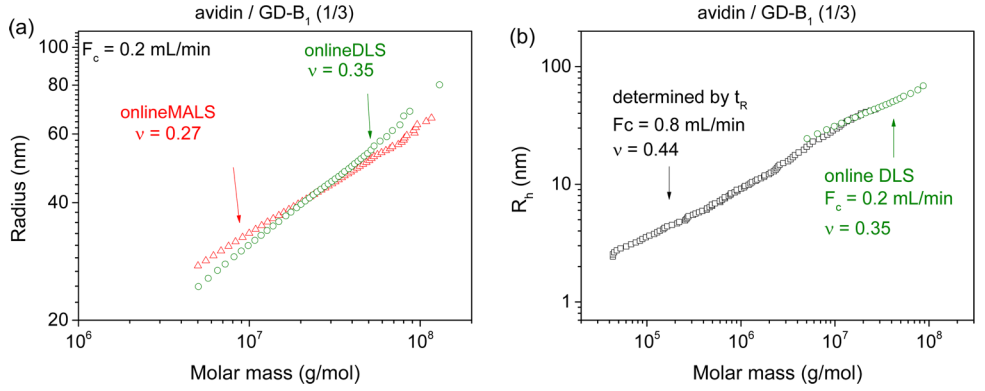

Figure 8. (a) Conformation plot with radii determined by online MALS (R_g, red triangles) and online DLS (R_h, green circles) as a function of molar mass with calculated scaling factors of biohybrid structures formed by avidin/GD-B_1 (1/3) determined by AF4-MALS-DLS (reduced F_c, separation method C) and (b) conformation plots of R_h with flow rates of F_c = 0.8 mL/min (black square, determined by t_R) and F_c = 0.2 mL/min (green triangles, determined by online DLS) of biohybrid structures formed by avidin/GD-B_1 (1/3).

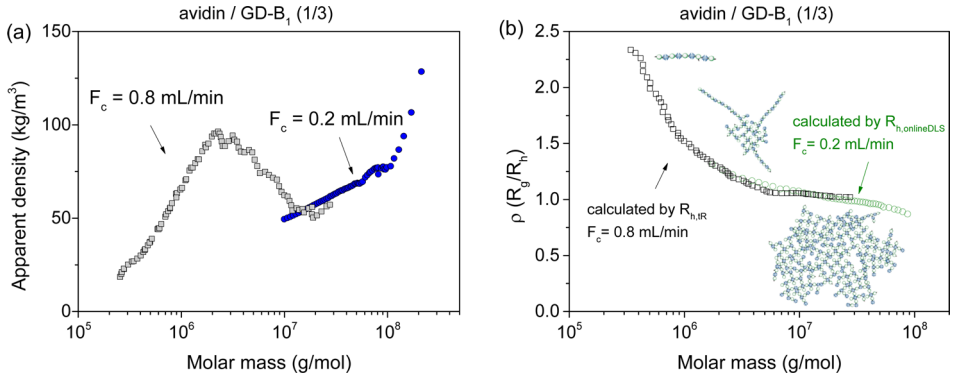

Figure 9. (a) Apparent density (calculated by R_g) and (b) ρ parameter vs molar mass; comparison of R_h determined at channel flow rates F_c = 0.8 mL/min (black squares, calculated by retention times) and F_c = 0.2 mL/min (green circles, determined by online DLS) of biohybrid structures formed by avidin/GD-B_1 (1/3).

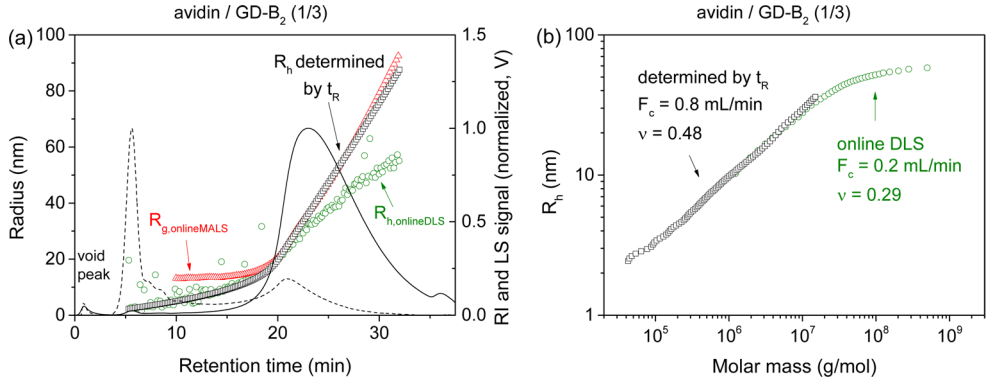

Figure 10. (a) AF4 fractograms (RI signal, dashed line; LS signal, solid line) with differently determined radii by online MALS (R_g, red triangle), by online DLS (R_h, green circles), and by retention times (R_h, black squares) relating to retention time and (b) conformation plots of R_h with flow rates of F_c = 0.8 mL/min (black squares, determined by t_R) and F_c = 0.2 mL/min (green circles, determined by online DLS) of biohybrid structures formed by avidin/GD-B_2 (1/3).

passive regulation of F_x. During these late stages of elution the actual cross-flow is in reality imprecise and lower than the stated 0.08 mL/min. Thus, the retention theory could not be applied for the determination of R_h. It should be noted, however, that separation still takes place (Supporting Information, Figure SI 10a), and detector results are valid. In order to avoid this limitation, care has to be taken that flows are monitored and regulated correctly during elution.

The conformation plots of large nanostructures of R_g and R_h are shown in Figure 8a.

The scaling factor ν of approximately 0.35 is typical for sphere-like structures. However, with the reduced flow larger sizes can be determined by both MALS and DLS. In Figure 8b, the conformation plots of differently determined R_h of different detector flow rate are overlaid. The obtained R_h data of the reduced F_c establish a consistent continuation of the R_h dependence determined by t_R at higher F_c, which shows that

DOI: 10.1021/acs.macromol.5b00824
Macromolecules 2015, 48, 4607−4619

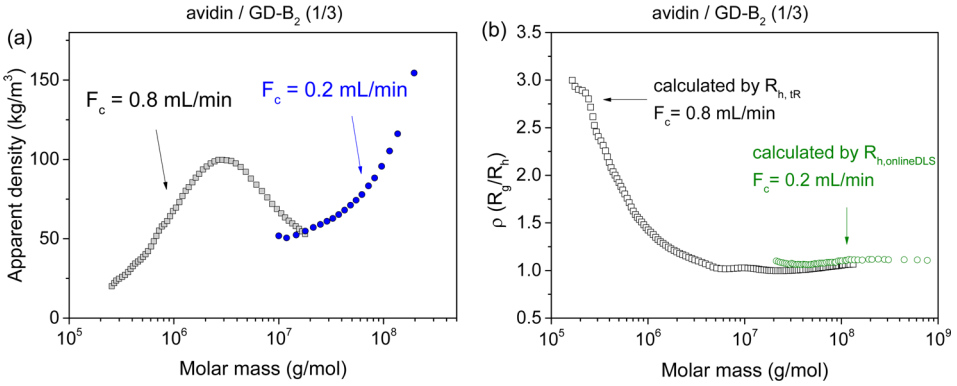

Figure 11. (a) Apparent density of R_g vs molar mass, comparison of η determined with varied flow rates F_c = 0.8 mL/min (gray squares) and F_c = 0.2 mL/min (blue circles) and (b) ρ parameters obtained by flow rates of F_c = 0.8 mL/min (black squares, determined by t_R) and F_c = 0.2 mL/min (green circles, determined by online DLS) of biohybrid structures formed by avidin/GD-B_2 (1/3).

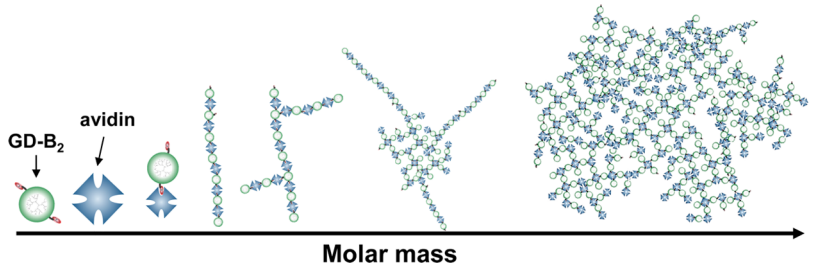

Figure 12. Schematic illustration of structure transformation (from 1D to 3D) of biohybrid structures formed by avidin and GD-B_2 (1/3) as a function of molar mass.

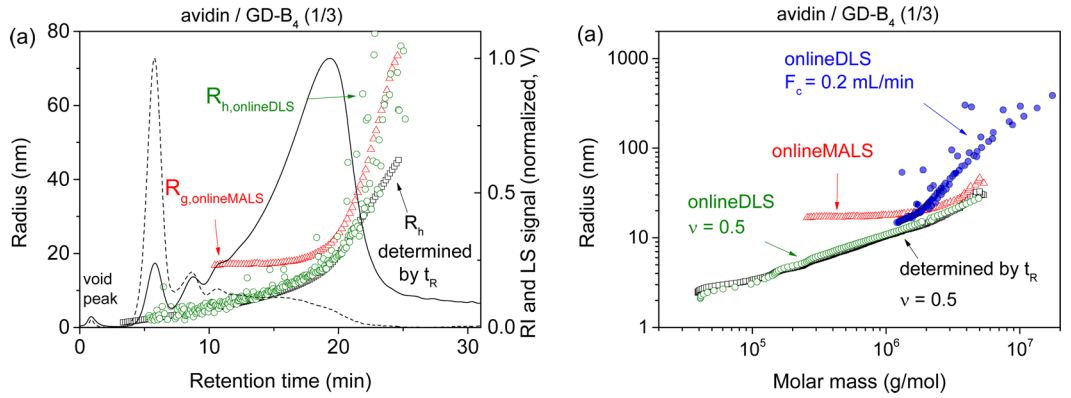

Figure 13. (a) AF4 fractograms (RI signal, dashed line; LS signal, solid line) with differently determined radii by online MALS (R_g, red triangles), by online DLS (R_h, green circles), and by retention times (R_h, black squares) relating to retention time and (b) conformation plots with differently determined radii as a function of molar mass with calculated scaling factors compared to results of reduced flow rates ($R_{h,onlineDLS}$, blue circles, F_c = 0.2 mL/min) of biohybrid structures formed by avidin/GD-B_4 (1/3).

larger particles indeed need more time for the detection of the diffusion coefficient.

The comparison of the apparent density (calculated by R_g with varied F_c) in Figure 9a shows that nanostructures with a molar mass of approximately 10^7 g/mol reach a second minimum in the density. For ultrahigh molar masses (above 10^7 g/mol) a further density increase was observed. Apparently, there is a coexistence of compact branched structures and loose networks. This assumption is in a good agreement with the trend of the ρ parameter (Figure 9b). A slight decrease to 0.8 is characteristic for sphere-like network structures.

Biohybrid Structures Based on GD-B_2 and GD-B_4. An increase of degree of biotinylation toward two biotin ligands (GD-B_2) leads to changes in the structural properties of the nanostructures. The comparison of fractograms of the R_h from online DLS and R_h from retention theory shows again a very good correlation (Figure 10a). In the region of late retention time and very large nanostructures the same deviation of differently determined R_h, as described for GD-B_1 (Figure 5a), can be observed. The complete conformation plots of biohybrid structures formed by bivalent GD-B_2 (Supporting Information, Figure SI 11a) are similar to the previously shown tendencies for GD-B_1 (Figure 8b): stiff, rod-like, and one-dimensional structures in the lower molar mass region toward branched macromolecules and relatively compact, sphere-like, three-dimensional structures for the high molecular nanostructures caused.

DOI: 10.1021/acs.macromol.5b00824
Macromolecules 2015, 48, 4607−4619

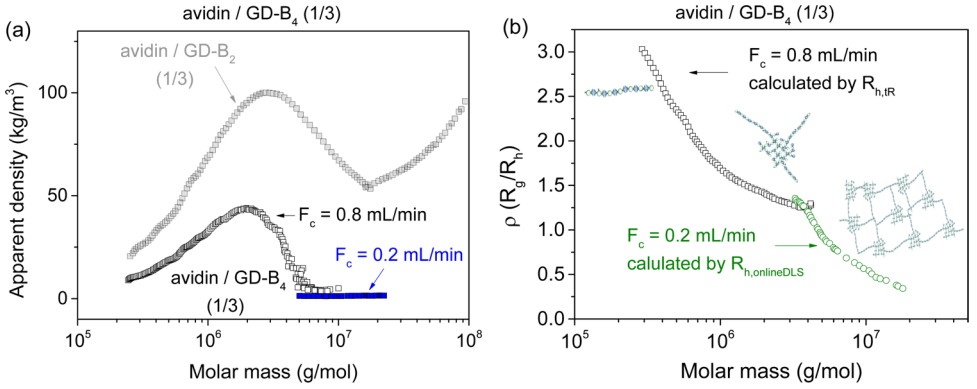

Figure 14. (a) Apparent density of R_g vs molar mass, comparison of η determined with varied flow rates F_c = 0.8 mL/min (black squares) and F_c = 0.2 mL/min (blue squares) of biohybrid structures formed by avidin/GD-B_2 (1/3; gray squares) and avidin/GD-B_4 (1/3) and (b) ρ parameters obtained by flow rates of F_c = 0.8 mL/min (black square, determined by t_R) and F_c = 0.2 mL/min (green circles, determined by online DLS) of biohybrid structures formed by avidin/GD-B_4 (1/3).

The lower R_h of online DLS is caused by low concentration and short acquisition times as explained above and a similar optimization of the measurement is required (Supporting Information, Figure SI 11b). Here, comparable tendency can be observed as described for biohybrid structures of GD-B_1. The R_h of online DLS (F_c = 0.2 mL/min) are a perfect continuation of the R_h curve determined by retention times (F_c = 0.8 mL/min) (Figure 10b). Compared to biohybrid structures formed by GD-B_1, the dimensions and the amount of nanostructures formed by GD-B_2 are significantly higher.

Furthermore, the calculated ρ parameters of the biohybrid structures formed by an excess of GD-B_2 (molar ratio 1/3) show a similar trend of reaching a constant value of ρ = 1. The structural changes become obvious by consideration of the apparent densities (Figure 11). With increasing molar masses the apparent density increases again as also observed for biohybrid structures formed by monovalent GD-B_1. With molar masses higher than 10^7 g/mol the network structures become denser. This is caused by the higher number of biotin ligands on the surface of GD and the higher probability to induce a branched network based on avidin binding capacity toward multivalent GD-B_x (see Figure 12).

Different trends are observed in the case of biohybrid structures formed by tetravalent GD-B_4. The comparison of differently determined R_h shows a good accordance between online DLS and calculation from retention theory (Figure 13a). Consequently, the conformation plots of differently determined R_h possess similar trends, too (Figure 13b). The scaling factors of 0.5 for R_h reveal an open structure over the entire molar mass region. The scaling behavior of R_g shows in the region of earlier retention times and/or molar masses a constant value. The R_g increases very rapidly with increased molar masses. The low concentration of ultrahigh molar mass nanostructures (above 5 × 10^6 g/mol) prevents an accurate online DLS detection. Therefore, the separation method was optimized as described in Experimental section (Supporting Information, Figure SI 12a). The obtained scaling plots (Supporting Information, Figure SI 12b) reveal at high molar masses (above 5 × 10^6 g/mol) a sphere-like shape. Compared to biohybrid structures formed by mono- and bivalent GD-B, the size of biohybrid structures of GD-B_4 at molar masses above 2 × 10^6 g/mol is significantly higher. This large size of nanostructures at comparable molar masses indicates a change in the conformation.

The calculated apparent density shows a similar trend depending on molar mass compared to the biohybrid structures formed by GD-B_2 (see Figure 14a). At molar masses of approximately 2 × 10^6 kg/mol the density reaches its maximum. However, the values are shifted to significantly reduced densities. The R_g determination with the reduced flow reveals very low apparent densities. Despite the presence of low apparent densities between 1 and 2 kg/m^3 at high molar significant higher molecular sizes are also observed. These differences can be explained by the ρ parameter calculated by R_h from retention times (F_c = 0.8 mL/min) and online DLS (for reduced flow) as a function of molar mass (Figure 14b). The first part of the curve is characterized by a very high starting point of 3, similar to the previous observations. In the same way, the molecular structure changes from stiff rods to branched structures toward network-like structures. In contrast to biohybrid structures of GD-B_1 and GD-B_2 the ρ parameter shows a further decrease down to 0.3. This very low value is typical for microgels[58] as observed for e.g. cereal β-glucans.[61] The nanostructures can be described as a loose network of linked, star-like macromolecules with highly branched cores and long, stiff segments. This is a sensible explanation following the large sizes and low densities of the nanostructures.

4. CONCLUSION

The main focus of this study was the application of AF4 for a comprehensive investigation of the structural and topological properties of biohybrid structures formed by biotinylated glycodendrimers and avidin. The AF4 in combination with MALS and DLS detection was the most convenient separation technique to characterize the multicomponent system consisting of well-defined bioconjugation adducts as well as complex biohybrid structures (nanostructures) and nonconverted initial compounds. The determination of molar masses and radii (R_g and R_h) by AF4-MALS-DLS led to an extensive characterization of the biohybrid structures on the molecular level. Therefore, two different strategies (by online DLS and by application of retention theory) for the calculation of R_h are compared. For the narrowly distributed initial compounds and well-defined conjugation adducts both strategies provided comparable results. At usually applied flow rates, deviations between both strategies became obvious in the high molar mass region. While the R_h calculation by retention times leads to reliable data, the online DLS delivers underestimated radii. An

DOI: 10.1021/acs.macromol.5b00824
Macromolecules 2015, 48, 4607−4619

optimization of the separation method provides realistic R_h values via DLS detection.

The conformational properties of the biohybrid structures, especially the nanostructures, are highly complex possessing morphological molar mass dependency. The molar ratio between GD-B_x and avidin plays an important role in the size of the formed biohybrid structures. An excess of GD-B leads to larger structures due to higher number of multivalent GD-B_x. Changes in the apparent density and ρ parameter (ratio of R_g and R_h) demonstrated a strong dependence of conformation, molar mass, and degree of biotinylation.

Biohybrid structures with molar masses up to 10^6 g/mol exhibit a stiff, rod-like structure (one-dimensional). With increased molar mass the morphology changes to branched and star-like structures (three-dimensional) with a very compact core and linear segments reaching into the outer surroundings. For ultrahigh molar masses (>10^7 g/mol) a further structural transformation is obvious. A higher density revealed coexistence of compact branched and loose network-like structures (three-dimensional). This large variation in the biohybrid topological diversity is highlighted in Figure 12. Another transformation of conformation behavior is existent in the case biohybrid structures formed by tetravalent GD-B_4. Here, molar masses above 2 × 10^6 g/mol possess less dense, microgel-like structure.

■ ASSOCIATED CONTENT

Supporting Information

DLS experiments in batch of initial compounds and biohybrid structures, influence of AF4 parameters (concentration, sample load, and focus), additional AF4 fractograms, AF4-MALS-DLS data of all biohybrid structures, studies on controlled formation of defined bioconjugates, and additional scaling properties. The Supporting Information is available free of charge on the ACS Publications website at DOI: 10.1021/acs.macromol.5b00824.

■ AUTHOR INFORMATION

Corresponding Authors

*E-mail lederer@ipfdd.de (A.L.).
*E-mail applhans@ipfdd.de (D.A.).
*E-mail lars.nilsson@food.lth.se (L.N.).

Notes

The authors declare no competing financial interest.

■ REFERENCES

(1) Chabre, Y. M.; Roy, R. *Chem. Soc. Rev.* **2013**, *42*, 4657−4708.
(2) Wu, Y.; Ng, D. Y. W.; Kuan, S. L.; Weil, T. *Biomater. Sci.* **2015**, 214−230.
(3) Imberty, A.; Chabre, Y. M.; Roy, R. *Chem.—Eur. J.* **2008**, *14*, 7490−7499.
(4) Lutz, J.-F.; Börner, H. G. *Prog. Polym. Sci.* **2008**, *33*, 1−39.
(5) Cosnier, S. *Biosens. Bioelectron.* **1999**, *14*, 443−456.
(6) Thordarson, P.; Le Droumaguet, B.; Velonia, K. *Appl. Microbiol. Biotechnol.* **2006**, *73*, 243−254.
(7) Ennen, F.; Boye, S.; Lederer, A.; Cernescu, M.; Komber, H.; Brutschy, B.; Voit, B.; Appelhans, D. *Polym. Chem.* **2014**, *5*, 1323−1339.
(8) Morgner, N.; Barth, H. D.; Brutschy, B.; Scheffer, U.; Breitung, S.; Gobel, M. *J. Am. Soc. Mass Spectrom.* **2008**, *19*, 1600−1611.
(9) Wattenberg, A.; Sobott, F.; Barth, H. D.; Brutschy, B. *Int. J. Mass Spectrom.* **2000**, *203*, 49−57.
(10) Wang, X. J.; Liu, L.; Luo, Y.; Zhao, H. Y. *Langmuir* **2009**, *25*, 744−750.
(11) Gu, Z. Y.; Patterson, G.; Cao, R.; Armitage, B. *J. Polym. Sci., Part B: Polym. Phys.* **2003**, *41*, 3037−3046.
(12) Krishna, O. D.; Wiss, K. T.; Luo, T.; Pochan, D. J.; Theato, P.; Kiick, K. L. *Soft Matter* **2012**, *8*, 3832−3840.
(13) Ke, S.; Wright, J. C.; Kwon, G. S. *Bioconjugate Chem.* **2007**, *18*, 2109−2114.
(14) Ke, S.; Wright, J. C.; Kwon, G. S. *Bioconjugate Chem.* **2007**, *18*, 1644−1650.
(15) Green, N. M. *Spectrophotometric Determination of Avidin and Biotin.* **1970**, *18* (Part A), 418−424.
(16) Harding, S. E.; Sattelle, D. B.; Bloomfiled, V. A. *Laser Light Scattering in Biochemistry*; Royal Society of Chemistry: London, 1992.
(17) Some, D. *Biophys. Rev.* **2013**, *5*, 147−158.
(18) Erber, M.; Boye, S.; Hartmann, T.; Voit, B. I.; Lederer, A. *J. Polym. Sci., Polym. Chem.* **2009**, *47*, 5158−5168.
(19) Li, Y.; Meunier, D. M.; Partain, E. M. *J. Chromatogr. A* **2014**, *1359*, 182−188.
(20) Pasch, H.; Makan, A.; Chirowodza, H.; Ngaza, N.; Hiller, W. *Anal. Bioanal. Chem.* **2014**, *406*, 1585−1596.
(21) Vilaplana, F.; Gilbert, R. G. *J. Sep. Sci.* **2010**, *33*, 3537−3554.
(22) Cave, R. A.; Seabrook, S. A.; Gidley, M. J.; Gilbert, R. G. *Biomacromolecules* **2009**, *10*, 2245−2253.
(23) Wahlund, K. G.; Giddings, J. C. *Anal. Chem.* **1987**, *59*, 1332−1339.
(24) Rebolj, K.; Pahovnik, D.; Zagar, E. *Anal. Chem.* **2012**, *84*, 7374−7383.
(25) Boye, S.; Polikarpov, N.; Appelhans, D.; Lederer, A. *J. Chromatogr. A* **2010**, *1217*, 4841−4849.
(26) Ashby, J.; Schachermeyer, S.; Duan, Y.; Jimenez, L. A.; Zhong, W. *J. Chromatogr. A* **2014**, *1358*, 217−224.
(27) di Cagno, M.; Terndrup Nielsen, T.; Lambertsen Larsen, K.; Kuntsche, J.; Bauer-Brandl, A. *Int. J. Pharm.* **2014**, *468*, 258−263.
(28) Schachermeyer, S.; Ashby, J.; Zhong, W. *J. Chromatogr. A* **2013**, *1295*, 107−113.
(29) Ma, P. L.; Buschmann, M. D.; Winnik, F. M. *Anal. Chem.* **2010**, *82*, 9636−9643.
(30) Roessner, D.; Kulicke, W. M. *J. Chromatogr. A* **1994**, *687*, 249−258.
(31) Makan, A. C.; Otte, T.; Pasch, H. *Macromolecules* **2012**, *45*, 5247−5259.
(32) Rolland-Sabaté, A.; Guilois, S.; Grimaud, F.; Lancelon-Pin, C.; Roussel, X.; Laguerre, S.; Viksø-Nielsen, A.; Putaux, J.-L.; D'Hulst, C.; Potocki-Véronèse, G.; Buléon, A. *Anal. Bioanal. Chem.* **2014**, *406*, 1607−1618.
(33) Rolland-Sabaté, A.; Guilois, S.; Jaillais, B.; Colonna, P. *Anal. Bioanal. Chem.* **2011**, *399*, 1493−1505.
(34) Ciric, J.; Rolland-Sabaté, A.; Guilois, S.; Loos, K. *Polymer* **2014**, *55*, 6271−6277.
(35) Pitkanen, L.; Striegel, A. M. *Analyst* **2014**, *139*, 5843−5851.
(36) Mathaes, R.; Winter, G.; Engert, J.; Besheer, A. *Int. J. Pharm.* **2013**, *453*, 620−629.
(37) Petersen, K.; Manangon, E.; Hood, J.; Wickline, S.; Fernandez, D.; Johnson, W.; Gale, B. *Anal. Bioanal. Chem.* **2014**, *406*, 7855−7866.
(38) John, C.; Langer, K. *J. Chromatogr. A* **2014**, *1346*, 97−106.
(39) Till, U.; Gaucher-Delmas, M.; Saint-Aguet, P.; Hamon, G.; Marty, J. D.; Chassenieux, C.; Payre, B.; Goudouneche, D.; Mingotaud, A. F.; Violleau, F. *Anal. Bioanal. Chem.* **2014**, *406*, 7841−7853.
(40) Einstein, A. *Ann. Phys.* **1906**, *324*, 289−306.
(41) Rolland-Sabaté, A.; Guilois, S.; Jaillais, B.; Colonna, P. *Anal. Bioanal. Chem.* **2011**, *399*, 1493−1505.
(42) Wittgren, B.; Wahlund, K. G. *J. Chromatogr. A* **1997**, *760*, 205−218.
(43) Moon, M. H.; Giddings, J. C. *J. Pharm. Biomed. Anal.* **1993**, *11*, 911−920.
(44) Nilsson, L.; Leeman, M.; Wahlund, K.-G.; Bergenståhl, B. *Biomacromolecules* **2006**, *7*, 2671−2679.
(45) Håkansson, A.; Magnusson, E.; Bergenståhl, B.; Nilsson, L. *J. Chromatogr. A* **2012**, *1253*, 120−126.

DOI: 10.1021/acs.macromol.5b00824
Macromolecules 2015, 48, 4607−4619

(46) Magnusson, E.; Håkansson, A.; Janiak, J.; Bergenståhl, B.; Nilsson, L. *J. Chromatogr. A* **2012**, *1253*, 127−133.
(47) Wahlund, K. G. *J. Chromatogr. A* **2013**, *1287*, 97−112.
(48) Runyon, J. R.; Nilsson, L.; Ulmius, M.; Castro, A.; Ionescu, R.; Andersson, C.; Schmidt, C. *Anal. Bioanal. Chem.* **2014**, *406*, 1597−1605.
(49) Glantz, M.; Håkansson, A.; Månsson, H. L.; Paulsson, M.; Nilsson, L. *Langmuir* **2010**, *26*, 12585−12591.
(50) Berry, G. C. *J. Chem. Phys.* **1966**, *44*, 4550.
(51) Boye, S.; Appelhans, D.; Boyko, V.; Zschoche, S.; Komber, H.; Friedel, P.; Formanek, P.; Janke, A.; Voit, B. I.; Lederer, A. *Biomacromolecules* **2012**, *13*, 4222−4235.
(52) Runyon, J. R.; Ulmius, M.; Nilsson, L. *Colloids Surf., A* **2014**, *442*, 25−33.
(53) Mullen, D. G.; Fang, M.; Desai, A.; Baker, J. R.; Orr, B. G.; Banaszak Holl, M. M. *ACS Nano* **2010**, *4*, 657−670.
(54) Han, H. J.; Sebby, K. B.; Singel, D. J.; Cloninger, M. J. *Macromolecules* **2007**, *40*, 3030−3033.
(55) Samuelson, L. E.; Sebby, K. B.; Walter, E. D.; Singel, D. J.; Cloninger, M. J. *Org. Biomol. Chem.* **2004**, *2*, 3075−3079.
(56) Sebby, K. B.; Walter, E. D.; Usselman, R. J.; Cloninger, M. J.; Singel, D. J. *J. Phys. Chem. B* **2011**, *115*, 4613−4620.
(57) Sinha, B. K.; Chignell, C. F. The synthesis and use of spin-labeled analogs of biotin in the study of avidin. In *Methods in Enzymology*; Donald, B., McCormick, L. D. W., Eds.; Academic Press: New York, 1979; Vol. *62*, pp 295−308.
(58) Burchard, W. Solution properties of branched macromolecules. In *Branched Polymers II*; Springer-Verlag: Berlin, 1999; Vol. *143*, pp 113−194.
(59) Coviello, T.; Kajiwara, K.; Burchard, W.; Dentini, M.; Crescenzi, V. *Macromolecules* **1986**, *19*, 2826−2831.
(60) Rojas, C. C.; Wahlund, K.-G.; Bergenståhl, B.; Nilsson, L. *Biomacromolecules* **2008**, *9*, 1684−1690.
(61) Håkansson, A.; Ulmius, M.; Nilsson, L. *Carbohydr. Polym.* **2012**, *87*, 518−523.

DOI: 10.1021/acs.macromol.5b00824
Macromolecules 2015, 48, 4607−4619